Available online at www.sciencedirect.com
ScienceDirect
Journal of Sound and Vibration 318 (2008) 911–926
JOURNAL OF SOUND AND VIBRATION
www.elsevier.com/locate/jsvi

Dynamic identification of structural systems with viscous and friction damping

Nicholas D. Oliveto, Giovanni Scalia, Giuseppe Oliveto*

Department of Civil and Environmental Engineering, Division of Structural Engineering, University of Catania, Italy

Received 20 September 2007; received in revised form 10 April 2008; accepted 15 April 2008
Handling Editor: C.L. Morfey
Available online 6 June 2008

Abstract

The response function of a dynamic system with viscous and friction damping is derived in the time domain and in the frequency domain, under a prescribed initial displacement. The response function in the frequency domain appears as the summation of three terms, each associated to a particular physical parameter of the dynamical system. Each of these functions is then used as a building block for an approximation function, which is used in an iteration procedure to identify the physical parameters of the dynamical system considered. At first, the solution in the frequency domain to a set of parameters, including the initial condition, is used as data for an identification procedure based on the least squares method. It is shown that the identification procedure provides the exact physical parameters of the system, including the initial displacement. Then an approximation to the frequency response function (FRF) is calculated through Discrete Fourier Transform (DFT) from the exact time response and is used in the identification procedure. The identified parameters are only an approximation, though a good one, to the original ones because of the errors introduced in the FRF by the DFT. Finally the procedure is applied to real acceleration data recorded during free-vibration tests on a base-isolated building. In spite of problems related to the complex nature of damping and stiffness in isolation systems with coupled sliding and rubber bearings, the identified parameters are reasonable and compare favourably with values obtained by other methods.

1. Introduction

Dynamic identification is a topic in structural dynamics whereby the dynamic characteristics of structural systems are estimated by means of experimental tests and suitable dynamical models. Popular textbooks on structural dynamics contain chapters and applications where methods are given on how to evaluate natural frequencies and damping ratios of actual structures [1,2], but specialized literature on structural identification is also available [3–8]. Extensive literature also exists on the identification of buildings and bridges under ambient and earthquake excitation [9–11]. Among the parameters to be identified are undamped frequencies of vibration, damping ratios and normal modes of vibration. These references to existing work are not meant

*Corresponding author. Tel.: +39 957382258; fax: +39 957382297.
E-mail address: goliveto@dica.unict.it (G. Oliveto).

0022-460X/$ - see front matter © 2008 Elsevier Ltd. All rights reserved.
doi:10.1016/j.jsv.2008.04.026

to be an exhaustive literature review on the topic but only aim at providing a proper setting for the present work.

Some structural systems are characterized by both viscous type damping and by friction type damping. Among those are some base-isolated buildings using laminated rubber isolators coupled with sliding isolators. In this case, viscous damping comes from the first type of isolator while friction damping comes from the second type. This type of base isolation has been used in Italy [12,13], and in Japan [14,15].

On base-isolated buildings, free-vibration tests are more easily performed than harmonic tests. In fact, due to the low-fundamental frequency of the isolated building and to the large initial stiffness due to friction, it is difficult to excite harmonically such a building; the harmonic actuator would be too large and cumbersome. Instead it is quite easy to perform a free-vibration test whereby the building is subjected to an imposed displacement and then is suddenly released. Several such tests have been performed in Italy [12,13] and in Japan [16]. The main parameters that need to be evaluated for the dynamic identification of the isolation mode [2], of a base-isolated building with laminated rubber bearings and sliding bearings are the initial displacement, the natural frequency, the viscous damping ratio, the dynamic friction force and the residual displacement. Although the initial displacement is usually imposed and therefore known in advance, its evaluation from system identification may represent a suitable check on the reliability of the identification procedure. The natural frequency, or equivalently the natural period, is usually amplitude dependent and only an average value may be determined. Most important is the evaluation of the viscous damping ratio which allows the separation of the amount of damping in the rubber bearings from that in the sliding bearings. The evaluation of the dynamic friction force in the sliding isolators and of the residual displacement completes the overall picture.

The object of the present paper is to develop a simple mechanical model which, on the basis of the measured acceleration, allows one to evaluate the above mentioned dynamical parameters in the frequency domain. The procedure in the time domain shown in Ref. [8] does not seem applicable to acceleration records derived from tests on continuous or multidegree of freedom systems such as base-isolated buildings. The identification procedure is initially tested on a theoretical problem, that is a problem with a known analytical solution, then the theoretically generated acceleration is used to calculate numerically its counterpart in the frequency domain. This is done in order to be able to have some confidence in the identification procedure in real life conditions, when the response acceleration is known as a time series and a Fourier Transform can only be evaluated numerically. Finally the identification procedure is tested using acceleration data recorded during free-vibration tests on one of the Solarino buildings [12,13]. Because the main purpose of the present study is the characterization of the isolation mode [2], the recorded acceleration is first treated to remove low frequency spurious components and short lived high-frequency components associated with the structural modes and with other disturbances [17].

That higher modes have a negligible effect in the identification of the isolation system may be shown by the modal expansion of the spatial distribution of inertia forces [2]. Because the deformation of the isolation bearings is dependent on the base shear which in turn depends on the inertia forces, it is the relative importance of the modal base shears to rule the effect on the dynamic behaviour of the isolation system. An example shown in Ref. [2] sets the second mode contribution to about 2% of that of the first mode, with higher modes of quickly decreasing importance. Calculations performed specifically for the Solarino building have shown even smaller contributions of the second and higher modes in the order of a few units in a thousand [18].

2. System considered

For the sake of simplicity, a single degree of freedom system is considered, although it is implied that this can represent the modal behaviour of a multidegree of freedom system. This system is shown in Fig. 1, where the main mechanical ingredients are a mass m, a linear spring characterized by a constant stiffness k, a dashpot with viscous damping coefficient c, a friction device applying a dynamic friction force f_{ad}. In addition to the above parameters, a static friction force f_{as} and a static external force f_0, needed to apply the initial displacement u_0, must be considered. The force–displacement relationship for the dynamic friction force is also shown in Fig. 1.

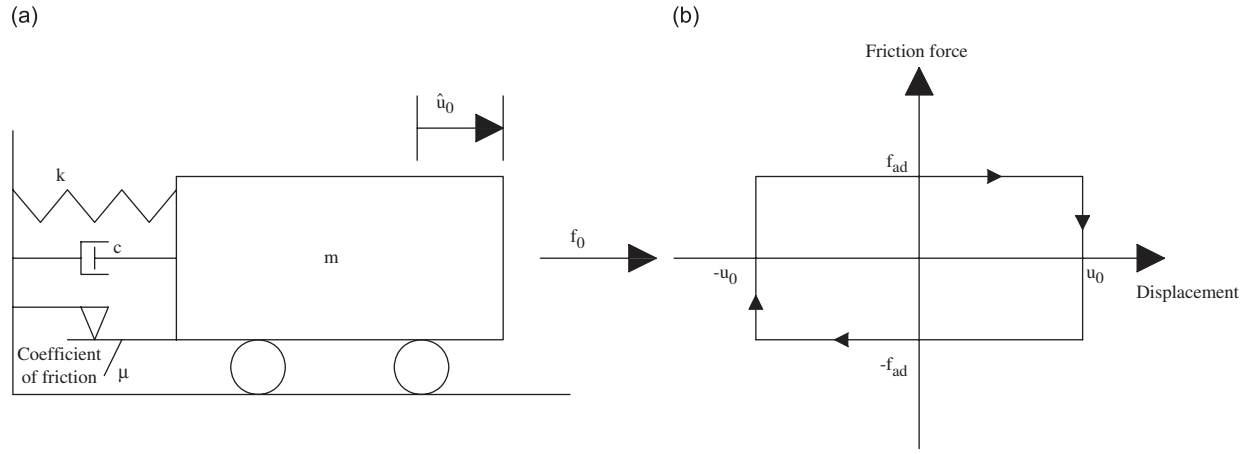

Fig. 1. (a) SDOF system considered, (b) friction force–displacement relationship.

3. Equation of motion

The equation of motion for the free vibration of the system shown in Fig. 1 may be written as follows:

$$m\ddot{u} + c\dot{u} + ku + f_{as}H(-t) + f_{ad}H(t)\mathrm{sgn}(\dot{u}_o) + 2\sum_{j=1}^{N} f_{ad}H(t-t_j)\mathrm{sgn}(\dot{u}_j) - f_{ad}H(t-t_r)\mathrm{sgn}(\dot{u}_N)$$
$$= f_0 H(-t) + f_{ar}H(t-t_r)\mathrm{sgn}(u_r) \tag{1}$$

where $H(t)$ is the Heaviside function, times t_j are the time instants when the velocity vanishes and the dynamic friction force changes sign, and t_r is the time when the system comes to a rest. The fourth term on the left-hand side of Eq. (1) represents the static friction force, which vanishes when the system is released, the fifth term represents the dynamic friction force which replaces the static one when the motion starts. Successive sign changes in the dynamic friction force are accounted for in each term in the summation, while the last term on the left-hand side expresses the last jump in the dynamic friction force before the system comes to a rest. The velocity argument in the sign functions always refers to the velocity just after the sign change. The static force f_0 on the right-hand side of Eq. (1) suddenly vanishes at time $t = 0$, while the residual friction force f_{ar} appears at time t_r when the system comes to a rest, thus balancing the force in the elastic spring. The sign functions in Eq. (1) are used to provide the proper sign for the dynamic friction force and for the static residual force.

Dividing Eq. (1) by the mass m and making suitable rearrangements, the following equation is obtained:

$$\ddot{u} + 2\zeta\omega_n\dot{u} + \omega_n^2 u + \omega_n^2 u_{as}H(-t) + \omega_n^2 u_{ad}H(t)\mathrm{sgn}(\dot{u}_0) + 2\omega_n^2 u_{ad}\sum_{j=1}^{N} H(t-t_j)\mathrm{sgn}(\dot{u}_j)$$
$$- \omega_n^2 u_{ad}H(t-t_r)\mathrm{sgn}(\dot{u}_N) = \omega_n^2 u_0 H(-t) + \omega_n^2 u_r H(t-t_r) \tag{2}$$

where

$$u_{as} = \frac{f_{as}}{k}, \quad u_{ad} = \frac{f_{ad}}{k}, \quad u_0 = \frac{f_0}{k}, \quad u_r = \frac{f_{ar}}{k}\mathrm{sgn}(u_r), \quad \omega_n^2 = \frac{k}{m} \tag{3}$$

and the initial displacement is given by

$$\hat{u}_0 = u_0 - u_{as} \tag{4}$$

By taking the derivative of both sides of Eq. (2) one finds:

$$\dddot{u}+2\zeta\omega_n\ddot{u}+\omega_n^2\dot{u}-\omega_n^2u_{\rm as}\delta(-t)+\omega_n^2u_{\rm ad}\delta(t)\mathrm{sgn}(\dot{u}_0)+2\omega_n^2u_{\rm ad}\sum_{j=1}^{N}\delta(t-t_j)\mathrm{sgn}(\dot{u}_j)$$
$$-\omega_n^2u_{\rm ad}\delta(t-t_r)\mathrm{sgn}(\dot{u}_N)=-\omega_n^2u_0\delta(-t)+\omega_n^2u_r\delta(t-t_r) \tag{5}$$

where $\delta(t)$ is the Dirac δ function.

By taking the Fourier transforms of each term in Eq. (5) this becomes

$$\dddot{U}+2\zeta\omega_n\ddot{U}+\omega_n^2\dot{U}-\omega_n^2u_{\rm as}+\omega_n^2u_{\rm ad}\,\mathrm{sgn}(\dot{u}_{\rm o})+2\omega_n^2u_{\rm ad}\sum_{j=1}^{N}\exp\{-\mathrm{i}\omega t_j\}\mathrm{sgn}(\dot{u}_j)$$
$$-\omega_n^2u_{\rm ad}\exp\{-\mathrm{i}\omega t_r\}\mathrm{sgn}(\dot{u}_N)=-\omega_n^2u_0+\omega_n^2u_r\exp\{-\mathrm{i}\omega t_r\} \tag{6}$$

and by using the following relationships between the derivatives of Fourier transforms:

$$\dddot{U}(\omega)=\mathrm{i}\omega\ddot{U}(\omega),\quad \dot{U}(\omega)=\frac{\ddot{U}(\omega)}{\mathrm{i}\omega}=\mathrm{i}\omega U(\omega) \tag{7}$$

Eq. (6) takes the following form:

$$\frac{1}{\omega}\left[2\zeta\omega_n\omega-\mathrm{i}(\omega_n^2-\omega^2)\right]\ddot{U}(\omega)=\omega_n^2u_{\rm as}-\omega_n^2u_0-\omega_n^2u_{\rm ad}\,\mathrm{sgn}(\dot{u}_0)-2\omega_n^2u_{\rm ad}\sum_{j=1}^{N}\exp\{-\mathrm{i}\omega t_j\}\mathrm{sgn}(\dot{u}_j)$$
$$+\omega_n^2u_{\rm ad}\,\exp\{-\mathrm{i}\omega t_r\}\mathrm{sgn}(\dot{u}_N)+\omega_n^2u_r\,\exp\{-\mathrm{i}\omega t_r\} \tag{8}$$

4. Solution in the time domain

In the various expressions of the equation of motion above, the times t_j are not known in advance, unless the motion has been recorded. Because in this paper we want to check the identification procedure against an analytical solution, we briefly present this solution here. In the static phase, which precedes the time instant $t=0$, the solution is given by

$$u(t)=u_0-u_{\rm as}=\hat{u}_0\quad \forall t<0 \tag{9}$$

In the successive phases of motion, displacement and velocity take the following expressions:

$$u_k(t)=\left[(\hat{u}_0-u_{\rm ad})-\sum_{j=1}^{k-1}2u_{\rm ad}\,\exp\{\zeta\omega_nt_j\}\right]\exp\{-\zeta\omega_nt\}\left[\cos\,\omega_Dt+\frac{\zeta\omega_n}{\omega_D}\sin\,\omega_Dt\right]-u_{\rm ad}(-1)^k \tag{10}$$

$$\dot{u}_k(t)=-\left[(\hat{u}_0-u_{\rm ad})-\sum_{j=1}^{k-1}2u_{\rm ad}\,\exp\{\zeta\omega_nt_j\}\right]\frac{\omega_n}{\sqrt{1-\zeta^2}}\exp\{-\zeta\omega_nt\}\sin\,\omega_Dt \tag{11}$$

where $k=1,2,3,4\ldots$ represents the current phase of motion and $t_j=j(\pi/\omega_D)$ $(j=1,2,3\ldots)$ denotes successive times when the velocity of the system vanishes. The system comes to a rest whenever the following conditions are satisfied:

$$t_r=r\frac{\pi}{\omega_D},\quad |u(t_r)|=|u_r|\leqslant u_{\rm as} \tag{12}$$

In any phase of motion the acceleration may be evaluated using the following expression:

$$\ddot{u}_k(t)=\omega_n^2u_{\rm ad}(-1)^{k+1}-2\zeta\omega_n\dot{u}_k(t)-\omega_n^2u_k(t) \tag{13}$$

which is the equation of motion for the kth phase. The exponent $k+1$ accounts for the sign of the friction force, which is negative in the first phase and alternates in the subsequent phases. In this model it is assumed

that the amplitude of the dynamic friction force remains constant during each phase of motion and changes only its sign from one phase to the next.

Once the displacements $\hat{u}_0$, u_{ad} and the mechanical parameters ω_n and ζ are known, the solution in terms of displacement, velocity and acceleration may be obtained using Eqs. (9)–(13).

5. Solution in the frequency domain

The solution in the frequency domain may be obtained from Eq. (8) in the following form:

$$\ddot{U}(\omega) = \ddot{\hat{U}}_0(\omega) + \ddot{U}_{ad}(\omega) + \ddot{U}_r(\omega) \tag{14}$$

where

$$\ddot{\hat{U}}_0(\omega) = -\frac{i\omega}{\omega_n^2 - \omega^2 + i2\zeta\omega_n\omega}\omega_n^2\hat{u}_0 \tag{15}$$

$$\ddot{U}_{ad}(\omega) = \frac{i\omega}{\omega_n^2 - \omega^2 + i2\zeta\omega_n\omega}\left[\exp\{-i\omega t_r\}\mathrm{sgn}(\dot{u}_N) - \mathrm{sgn}(\dot{u}_0) - 2\sum_{j=1}^{N}\exp\{-i\omega t_j\}\mathrm{sgn}(\dot{u}_j)\right]\omega_n^2 u_{ad} \tag{16}$$

$$\ddot{U}_r(\omega) = \frac{i\omega}{\omega_n^2 - \omega^2 + i2\zeta\omega_n\omega}[\exp\{-i\omega t_r\}]\omega_n^2 u_r \tag{17}$$

The solution in terms of velocity and displacement is easily obtained by using the standard relationships between derivatives of Fourier transforms, as is shown by Eq. (7).

In particular, the moduli of the functions $\ddot{\hat{U}}_0(\omega)$ and $\dot{\hat{U}}_0(\omega)$ take the following expressions:

$$\left|\ddot{\hat{U}}_0(\omega)\right| = \frac{\omega}{\sqrt{(\omega_n^2 - \omega^2)^2 + (2\zeta\omega_n\omega)^2}}\omega_n^2\hat{u}_0 \tag{18}$$

$$\left|\dot{\hat{U}}_0(\omega)\right| = \frac{\omega_n^2\hat{u}_0}{\sqrt{(\omega_n^2 - \omega^2)^2 + (2\zeta\omega_n\omega)^2}} \tag{19}$$

It is easy to show that the peak frequencies for $\left|\dot{\hat{U}}_0(\omega)\right|$ and $\left|\ddot{\hat{U}}_0(\omega)\right|$ are given by

$$\omega_V = \omega_n\sqrt{1 - 2\zeta^2} \tag{20}$$

$$\omega_A = \omega_n \tag{21}$$

These expressions are valuable because, when friction is negligible, they tell us that the natural frequency of the system coincides with the peak frequency of the acceleration (Eq. (21)) and the damping ratio may be obtained by solving Eq. (20). If friction is small, but not negligible, Eqs. (20) and (21) still provide good values for starting the identification procedure. We can anticipate that the starting values for the damping ratio and the natural frequency in the identification of the Solarino tests are obtained by means of Eqs. (20) and (21).

6. Sample solution

In this section we derive a sample solution to be used as a test function for the identification procedure that will be presented later. Let us take $\hat{u}_0 = 0.11\,\mathrm{m}$, $u_{ad} = 0.005\,\mathrm{m}$, $f_n = \omega_n/2\pi = 0.5\,\mathrm{Hz}$, $\zeta = 0.10$. The time domain solution, obtained by means of Eqs. (9)–(13), is shown in Fig. 2 in terms of acceleration. This solution provides the times $t_j = j(\pi/\omega_D)$, $(j = 1,2,3\ldots)$, when the velocity vanishes and the dynamic friction force changes sign, and also the residual displacement u_r. The actual values are given in Table 1. The sampling frequency has been set to 1000 Hz to be consistent with the sampling frequency of the dynamical tests performed on the Solarino building.

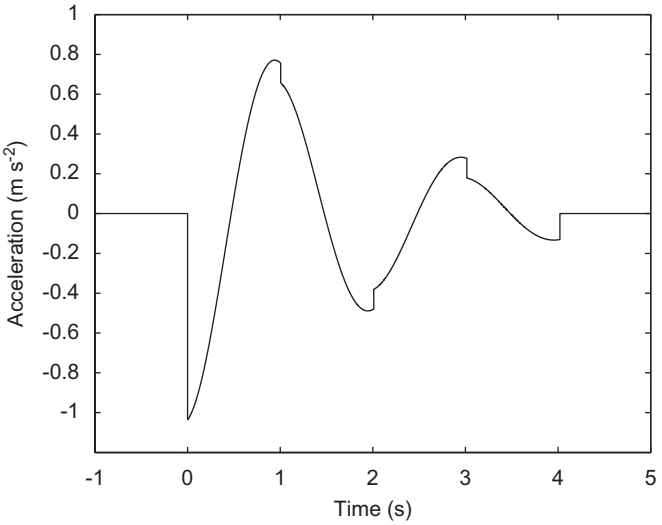

Fig. 2. Analytically generated acceleration sample.

Table 1
Characteristic times of the sample solution and residual displacement

t_1 (s)	t_2 (s)	t_3 (s)	t_r (s)	u_r (m)
1.0050	2.0101	3.0151	4.0202	0.0082

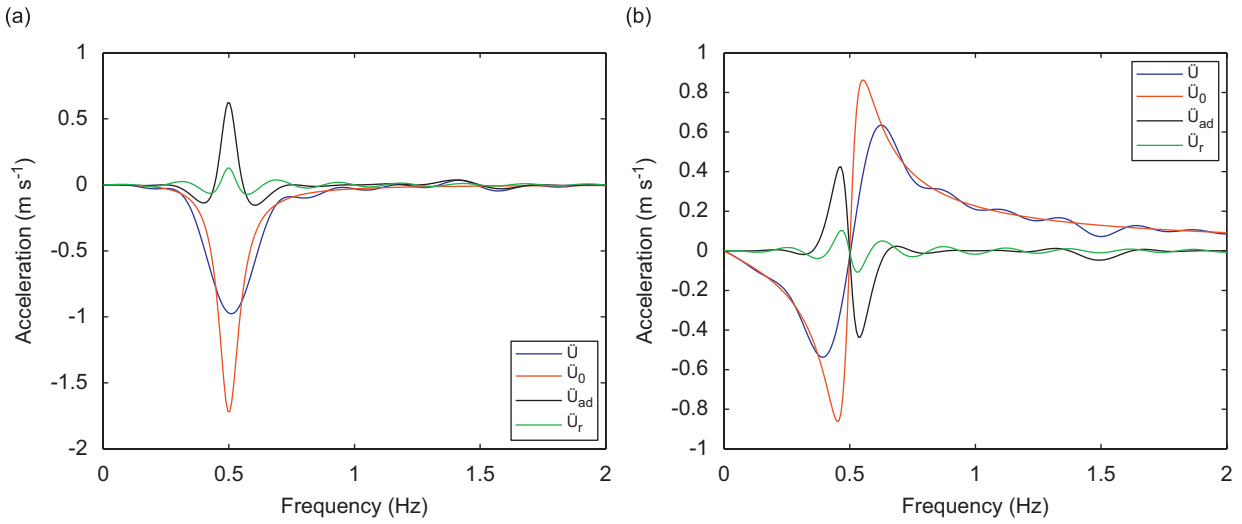

Fig. 3. Fourier transform $\ddot{U}$ of the acceleration sample shown in Fig. 2 and its components $\ddot{U}_0$, $\ddot{U}_{ad}$ and $\ddot{U}_r$: (a) real part, (b) imaginary part.

At this point, it is also possible to obtain the solution in the frequency domain by using Eqs. (14)–(17). This is shown in Fig. 3, as well as the three right-hand side terms from Eq. (14), thus providing a measure of the relative importance of each term.

7. Identification procedure

In this section we assume that the Fourier transform of the sample solution shown in Fig. 2 can be calculated analytically. We shall use this function to identify all the system parameters which allow one to calculate the time domain solution, that is $\hat{u}_0$, u_{ad}, u_r, ω_n and ζ. These parameters can be conveniently considered as the components of the following vector:

$$\mathbf{x} = (\hat{u}_0, u_{\mathrm{ad}}, u_r, \omega_n, \zeta) \tag{22}$$

The identification procedure will be based on the least squares method. The known function is denoted by $F_0(\omega)$ and the approximation function by $F(\omega)$. The latter may be expressed as the following linear combination of base functions:

$$F(\omega, \mathbf{x}) = \hat{u}_0 F_1(\omega, \mathbf{x}) + u_{\mathrm{ad}} F_2(\omega, \mathbf{x}) + u_r F_3(\omega, \mathbf{x}) \tag{23}$$

where the functions $F_1(\omega, \mathbf{x})$, $F_2(\omega, \mathbf{x})$ and $F_3(\omega, \mathbf{x})$ have the following expressions:

$$F_1(\omega, \mathbf{x}) = \frac{\ddot{\hat{U}}_0(\omega, \mathbf{x})}{\hat{u}_0}, \quad F_2(\omega, \mathbf{x}) = \frac{\ddot{U}_{\mathrm{ad}}(\omega, \mathbf{x})}{u_{\mathrm{ad}}}, \quad F_3(\omega, \mathbf{x}) = \frac{\ddot{U}_r(\omega, \mathbf{x})}{u_r} \tag{24}$$

The approximation function can be conveniently written in the following form:

$$\begin{aligned} F(\omega, \mathbf{x}) &= F(\omega, \tilde{\mathbf{x}}) + \left.\frac{\partial F}{\partial \hat{u}_0}\right|_{\tilde{x}} \left(\hat{u}_0 - \tilde{\hat{u}}_0\right) + \left.\frac{\partial F}{\partial u_{\mathrm{ad}}}\right|_{\tilde{\mathbf{x}}} (u_{\mathrm{ad}} - \tilde{u}_{\mathrm{ad}}) + \left.\frac{\partial F}{\partial u_r}\right|_{\tilde{\mathbf{x}}} (u_r - \tilde{u}_r) \\ &+ \left.\frac{\partial F}{\partial \omega_n}\right|_{\tilde{\mathbf{x}}} (\omega_n - \tilde{\omega}_n) + \left.\frac{\partial F}{\partial \zeta}\right|_{\tilde{\mathbf{x}}} (\zeta - \tilde{\zeta}) = F(\omega, \tilde{\mathbf{x}}) + F_1(\omega, \tilde{\mathbf{x}})\left(\hat{u}_0 - \tilde{\hat{u}}_0\right) + F_2(\omega, \tilde{\mathbf{x}})(u_{\mathrm{ad}} - \tilde{u}_{\mathrm{ad}}) \\ &+ F_3(\omega, \tilde{\mathbf{x}})(u_r - \tilde{u}_r) + F_4(\omega, \tilde{\mathbf{x}})(\omega_n - \tilde{\omega}_n) + F_5(\omega, \tilde{\mathbf{x}})(\zeta - \tilde{\zeta}) \end{aligned} \tag{25}$$

where the symbols with a $\sim$, collected in vector $\tilde{\mathbf{x}}$, denote the current values of the model parameters.

The two additional base functions defined below are introduced into the procedure by Eq. (25):

$$F_4(\omega, \tilde{\mathbf{x}}) = \left.\frac{\partial F}{\partial \omega_n}\right|_{\tilde{\mathbf{x}}} = \frac{2\omega^2 \tilde{\omega}_n \left(\mathrm{i}\omega + \tilde{\zeta}\tilde{\omega}_n\right)\left(\tilde{\hat{u}}_0 - A\tilde{u}_{\mathrm{ad}} - \exp\{-\mathrm{i}\omega t_r\}\tilde{u}_r\right)}{\left(\tilde{\omega}_n^2 - \omega^2 + \mathrm{i}2\tilde{\zeta}\tilde{\omega}_n\omega\right)^2} \tag{26}$$

$$F_5(\omega, \tilde{\mathbf{x}}) = \left.\frac{\partial F}{\partial \zeta}\right|_{\tilde{\mathbf{x}}} = \frac{2\omega^2 \tilde{\omega}_n^3 \left(-\tilde{\hat{u}}_0 + A\tilde{u}_{\mathrm{ad}} + \exp\{-\mathrm{i}\omega t_r\}\tilde{u}_r\right)}{\left(\tilde{\omega}_n^2 - \omega^2 + \mathrm{i}2\tilde{\zeta}\tilde{\omega}_n\omega\right)^2} \tag{27}$$

$$A = \exp\{-\mathrm{i}\omega t_r\}\mathrm{sgn}(\dot{u}_N) - \mathrm{sgn}(\dot{u}_0) - 2\sum_{j=1}^{N} \exp\{-\mathrm{i}\omega t_j\}\mathrm{sgn}(\dot{u}_j) \tag{28}$$

At this point the approximation function can be expressed more simply as follows:

$$F(\omega, \mathbf{x}) = \tilde{F} + \alpha_i \tilde{F}_i \quad (i = 1, 2 \ldots 5) \tag{29}$$

with α_i having the following expressions:

$$\alpha_1 = \hat{u}_0 - \tilde{\hat{u}}_0, \quad \alpha_2 = u_{\mathrm{ad}} - \tilde{u}_{\mathrm{ad}}, \quad \alpha_3 = u_r - \tilde{u}_r, \quad \alpha_4 = \omega_n - \tilde{\omega}_n, \quad \alpha_5 = \zeta - \tilde{\zeta} \tag{30}$$

For the functions $\tilde{F}_i(\omega, \mathbf{x})$ to be defined, the components of the $\tilde{\mathbf{x}}$ vector and the characteristic times t_j ($j = 1, 2, \ldots, N$) and t_r need to be specified. These times can be read from the known function in the time domain (for example from Fig. 2), while the initial values for the components of the $\mathbf{x}$ vector can be chosen arbitrarily within the expected range. The error, defined as the difference between the exact solution $F_0(\omega)$ and the approximate one $F(\omega, \mathbf{x})$, may be expressed in the following way:

$$e^2 = \langle F - F_0, \bar{F} - \bar{F}_0 \rangle = \left\langle \tilde{F} + \alpha_i \tilde{F}_i - F_0, \bar{\tilde{F}} + \alpha_i \bar{\tilde{F}}_i - \bar{F}_0 \right\rangle \tag{31}$$

where

$$\langle F(\omega,\mathbf{x}),\overline{F(\omega,\mathbf{x})}\rangle=\int_{-\infty}^{+\infty}F(\omega,\mathbf{x})\overline{F(\omega,\mathbf{x})}\,\mathrm{d}\omega \tag{32}$$

and a bar on top of a function denotes its complex conjugate.

Once the error has been defined, the least squares method can be applied, as shown by the expressions below:

$$\frac{\partial e^2}{\partial\alpha_k}=\left\langle\delta_{ik}\tilde{F}_i,\bar{\tilde{F}}+\alpha_j\bar{\tilde{F}}_j-\bar{F}_0\right\rangle+\left\langle\tilde{F}+\alpha_i\tilde{F}_i-F_0,\delta_{jk}\bar{\tilde{F}}_j\right\rangle=0 \tag{33}$$

$$\left\langle\tilde{F}_k,\bar{\tilde{F}}+\alpha_i\bar{\tilde{F}}_i-\bar{F}_0\right\rangle+\left\langle\tilde{F}+\alpha_i\tilde{F}_i-F_0,\bar{\tilde{F}}_k\right\rangle=0 \tag{34}$$

$$\left\langle\tilde{F}_k,\bar{\tilde{F}}-\bar{F}_0\right\rangle+\alpha_i\left\langle\tilde{F}_k,\bar{\tilde{F}}_i\right\rangle+\left\langle\tilde{F}-F_0,\bar{\tilde{F}}_k\right\rangle+\alpha_i\left\langle\tilde{F}_i,\bar{\tilde{F}}_k\right\rangle=0 \tag{35}$$

By noting that the following equalities hold,

$$\mathrm{Re}\left\langle\tilde{F}-F_0,\bar{\tilde{F}}_k\right\rangle=\mathrm{Re}\left\langle\bar{\tilde{F}}-\bar{F}_0,\tilde{F}_k\right\rangle=\mathrm{Re}\left\langle\tilde{F}_k,\bar{\tilde{F}}-\bar{F}_0\right\rangle \tag{36}$$

Eq. (35) can be written as

$$\mathrm{Re}\left\langle\tilde{F}_k,\bar{\tilde{F}}_i\right\rangle\alpha_i=\mathrm{Re}\langle\tilde{F}_k,\bar{F}_0\rangle-\mathrm{Re}\left\langle\tilde{F}_k,\bar{\tilde{F}}\right\rangle \tag{37}$$

Eq. (37) may be finally written in a more compact form as

$$A_{ki}\alpha_i=b_k\quad(k,i=1,2,\ldots,5) \tag{38}$$

where

$$A_{ki}=\mathrm{Re}\left\langle\tilde{F}_k,\bar{\tilde{F}}_i\right\rangle,\quad b_k=\mathrm{Re}\langle\tilde{F}_k,\bar{F}_0\rangle-\mathrm{Re}\left\langle\tilde{F}_k,\bar{\tilde{F}}\right\rangle \tag{39}$$

The solution of Eq. (38) provides a set of coefficients α_i $(i=1,2,\ldots,5)$. These give us an approximation of all the system parameters, thus allowing for the evaluation of the approximating function $F(\omega,\ \mathbf{x})$, which can then be used in Eq. (31) to calculate the error. Actually, a dimensionless form is used to evaluate the error, that is

$$e^2=\frac{\langle F-F_0,\bar{F}-\bar{F}_0\rangle}{\langle F_0,\bar{F}_0\rangle} \tag{40}$$

The current approximate values of the system parameters contained in vector $\mathbf{x}$ can be used for the evaluation of the new base functions $F_i(\omega,\mathbf{x})$, $(i=1,2,\ldots,5)$, and the procedure may be iterated. The iteration may be terminated when the error in Eq. (40) becomes less than a given tolerance.

Table 2
Performance of the identification procedure using the Analytical Fourier Transform of the sample solution

Tolerance ε	Iterations	$\hat{u}_0$ (m)	u_{ad} (m)	u_r (m)	ζ	f_n (Hz)
10^{-3}	19	0.1098	0.0049	0.0084	0.1004	0.4977
10^{-6}	20	0.1100	0.0050	0.0082	0.1001	0.4984
10^{-9}	24	0.1100	0.0050	0.0082	0.1000	0.4997
10^{-12}	28	0.1100	0.0050	0.0082	0.1000	0.4999
10^{-15}	33	0.1100	0.0050	0.0082	0.1000	0.5000

8. Numerical applications

In this section we apply the identification procedure presented above to the sample solution shown in Section 6. The starting values chosen for the components of the **x** vector are $u_0 = 0.15\,\text{m}$, $u_{\text{ad}} = 0.008\,\text{m}$, $u_r = 0.007\,\text{m}$, $f_n = 0.4\,\text{Hz}$ and $\zeta = 0.3$. The application of the procedure provides the results shown in Table 2. The cut-off frequency used to evaluate the integrals in Eq. (39) was 5 Hz.

It is clear from the observation of Table 2 that the procedure converges to the exact results, which are obtained after 33 iterations with a tolerance of 10^{-15}. However, the closer the starting values are chosen to the exact ones, the faster the procedure will converge.

9. Time series

In real applications, as in free vibration tests, the time domain acceleration is provided in the form of a recorded time series with a specified time step or sampling frequency. In such cases, an exact Fourier transform of the acceleration is not available. The usual approximation is in the form of a Discrete Fourier Transform (DFT), performed via the Fast Fourier Transform algorithm (FFT). These transforms nowadays can be performed easily and efficiently within a Matlab environment. In fact, the FFT is a typical Matlab function.

To see how the identification procedure previously described performs under a real life application, the analytically derived sample function has been sampled with a time step $\Delta t = 0.001\,\text{s}$, which corresponds to a sampling frequency $f_c = 1000\,\text{Hz}$. The time series so obtained has been transformed into the frequency domain by using the FFT algorithm. It is well known [19] that the DFT replaces an aperiodic function with a periodic one; the longer the period, the closer the periodic function gets to the aperiodic one. In the present application the number of sampled values is taken equal to $N = 2^{17} = 131{,}072$, which corresponds to a period $T = (N-1)\Delta t = 131{,}071 \times 10^{-3} = 131.071\,\text{s}$. Because the length of the non-zero segment of the considered acceleration is only $t_r = 4.0201\,\text{s}$, the remaining time interval is filled with zeros. Therefore, our time series is composed of 4021 sampled values followed by 127,050 zeros.

A comparison between the given aperiodic function and the assumed periodic one is shown in Fig. 4. The Fourier transform of the given aperiodic function is provided by Eq. (14) and has been shown in Fig. 3. The DFT of the approximating periodic function is shown in Fig. 5. In the frequency range considered and with the scale factor chosen, the DFT cannot be distinguished from the analytical Fourier transform shown in Fig. 3. However, as higher frequency ranges are considered, the difference between FT and DFT tends to

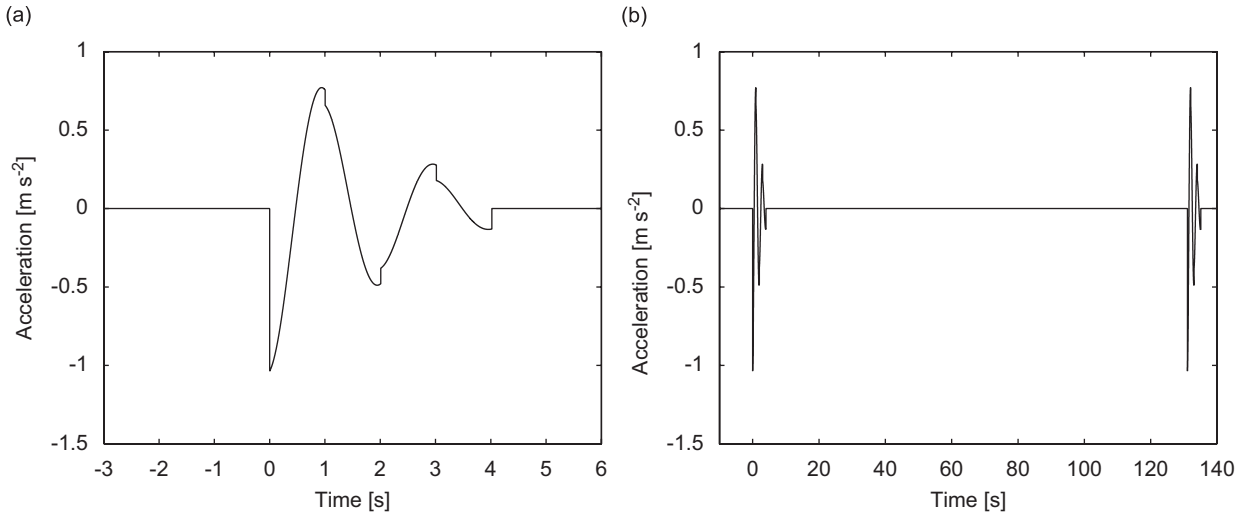

Fig. 4. (a) Aperiodic acceleration sample ($t_r = 4.02\,\text{s}$) and (b) corresponding periodic function ($T = 131.07\,\text{s}$).

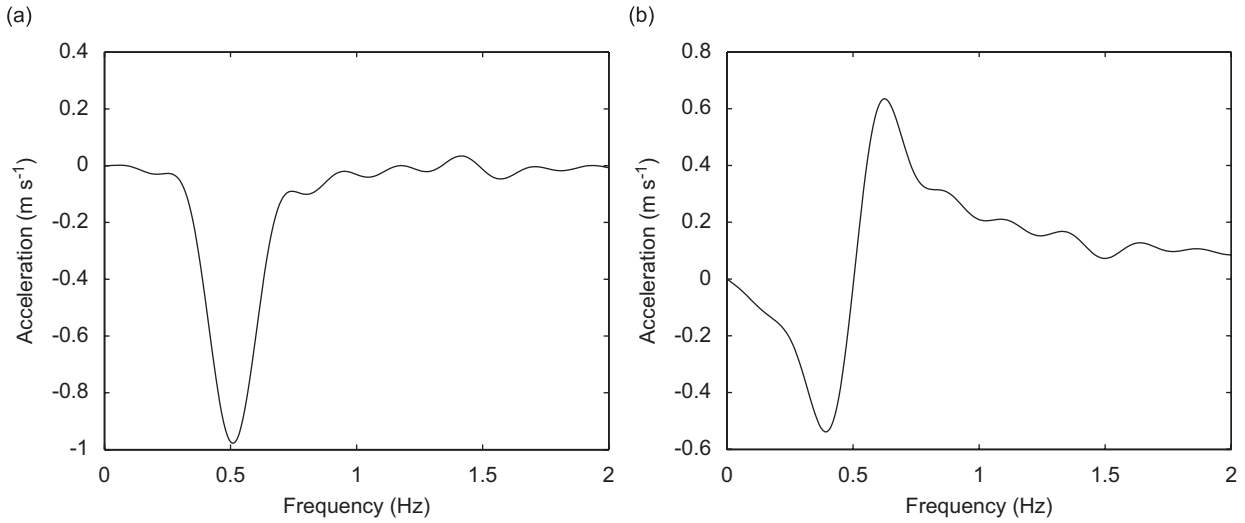

Fig. 5. Discrete Fourier transform of the acceleration function of Fig. 4 sampled at a frequency of 1000 Hz: (a) real part and (b) imaginary part.

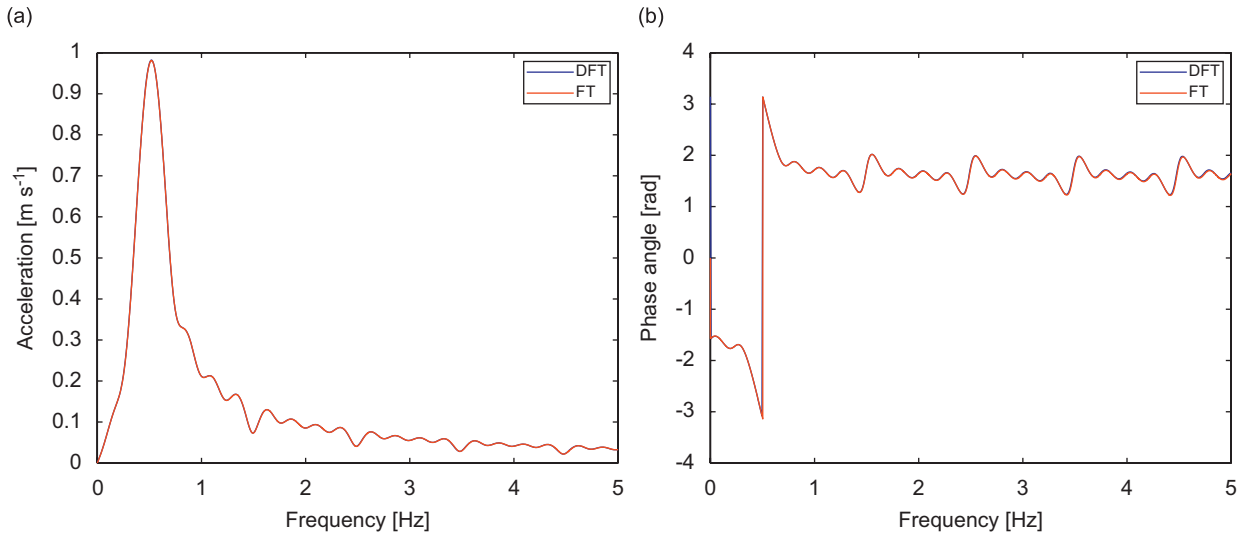

Fig. 6. Comparison between FT and DFT: (a) modulus, (b) phase angle.

become significant. Therefore when using the DFT to approximate the FT, the identification procedure should be carried out in a frequency range where the difference between the DFT and the FT is negligible.

10. Numerical applications with time series and DFT

In this section we shall consider numerical applications which simulate real life experiments. The acceleration function shown in Fig. 2 is sampled with a frequency of 1000 Hz and transformed into the frequency domain via DFT using the FFT algorithm. The result is shown in Fig. 6 in terms of modulus and phase angle in the frequency range 0–5 Hz. For comparison, in the same figure, the analytical Fourier transform of the original function is shown. At the scale used in the figure differences appear to be negligible.

Table 3
Performance of the identification procedure using the Discrete Fourier Transform of the sample solution

Tolerance ε	iterations	$\hat{u}_0$ (m)	u_{ad} (m)	u_r (m)	ζ	f_n (Hz)
10^{-3}	15	0.1099	0.0050	0.0076	0.0989	0.4981
10^{-5}	16	0.1102	0.0050	0.0083	0.1005	0.4987
Exact values		0.1100	0.0050	0.0082	0.1000	0.5000
Error (%)		0.18	0.00	1.22	0.50	−0.26

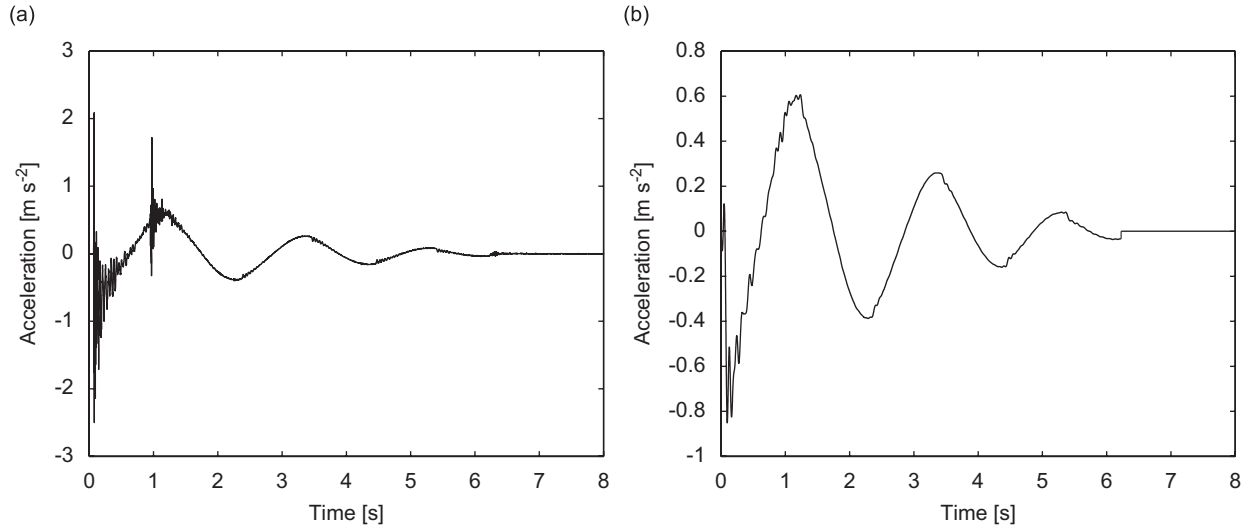

Fig. 7. Acceleration records from a Solarino building: (a) original record, (b) treated signal.

Some differences however may be noticed especially in the high-frequency tail of the graphs. The starting values chosen for the components of the **x** vector are the same as those used in Section 8. The results obtained with a cut-off frequency of 5 Hz are shown in Table 3.

The best results are obtained with an error tolerance $\varepsilon = 10^{-5}$ after 16 iterations. These come quite close to the assumed parameters, as can be seen by comparison with the exact values also shown in Table 3. The error on each of the identified parameters is defined as

$$e = \frac{p_i - p_e}{p_e} \times 100 \tag{41}$$

and is shown in the last row of Table 3.

The main result of this section consists in the realization that the discrete Fourier transform, necessary when dealing with time series, introduces errors in the identification results. However, these errors are not large and generally comparable with other engineering uncertainties.

11. Data from tests on the Solarino building

In this section the identification procedure is applied to the acceleration recorded during the free vibration tests performed on a four storey base-isolated building in the town of Solarino [12,13]. The acceleration recorded during the first dynamic test, on the second floor, roughly corresponding to the centre of mass of the building, is shown in Fig. 7. On the left-hand side the original record is shown, while the plot on the right-hand side shows the record after being treated for the removal of high-frequency components using wavelet decomposition [13,17]. The treated signal reproduces the main characteristics of the original record, except for

the irregular behaviour due to the high-frequency components. The high-frequency spikes towards the end of the first half period of motion in the original signal may be due to the impact of the base slab against the pushing and release device used in the tests.

One peculiar aspect of the treated signal, as well as of the original record, is the changing period with time. It may be expected that this characteristic will affect the performance of the identification procedure proposed in the previous sections. In fact, the model which is the foundation of the identification procedure assumes a constant period.

Although in principle the initial displacement could be included within the parameters to be identified, for the sake of obtaining more reliable results, the procedure has been adjusted assuming the initial displacement to be known. Actually, in a free vibration test the initial displacement is imposed and therefore given. In the case presented here it was 11.48 cm. This adjustment can be justified by the fact that a given acceleration history may correspond to different displacement histories, depending on initial values of displacement and velocity.

The starting values for the damping ratio and the natural frequency in the identification procedure are obtained by means of Eqs. (20) and (21), where ω_V and ω_A are the frequencies of the peaks of velocity and acceleration Fourier spectra of the recorded data. The acceleration spectrum is evaluated by FFT of the recorded acceleration while the velocity spectrum is obtained by applying the standard relationship between Fourier transforms of velocity and acceleration, as shown in Eqs. (7). By using this approach, the starting values of the identification procedure are $f_n = 0.4807\,\text{Hz}$ and $\zeta = 0.2663$, while $u_{\text{ad}} = 0.008\,\text{m}$ and $u_r = 0.007\,\text{m}$, were chosen with some engineering judgement equal to the values used in the analytical test. However, the procedure does not appear to be particularly sensitive to the starting values for ζ, u_{ad} and u_r, provided that these are kept within reasonable bounds. The times when the velocity vanishes must be also evaluated from the acceleration record. These correspond to the jumps in the acceleration, due to the change of sign in the friction force, and may be easily identified with some judgement. In the present case these times, identified from the data shown in Fig. 7 (b), are $t_1 = 1.233\,\text{s}$, $t_2 = 2.343\,\text{s}$, $t_3 = 3.377\,\text{s}$, $t_4 = 4.428\,\text{s}$, $t_5 = 5.363\,\text{s}$, $t_r = 6.226\,\text{s}$.

The identified system parameters obtained are:

$$u_{\text{ad}} = 0.0027\,\text{m}, \quad u_r = -0.0122\,\text{m}, \quad \zeta = 0.1190, \quad f_n = 0.4315\,\text{Hz}$$

A better understanding of the performance of the identification procedure may be obtained by comparison of the acceleration plots in the time domain, which are shown on the left-hand side of Fig. 8. The graph on the right-hand side of the same figure shows the error as a function of the number of iterations, giving an idea of

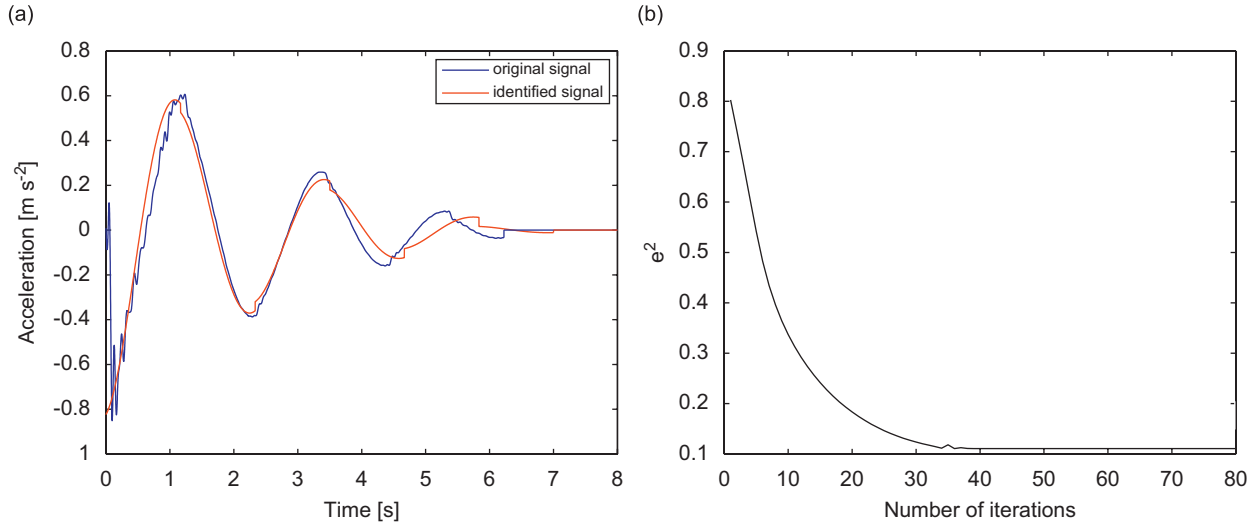

Fig. 8. (a) Original and identified signals, (b) convergence rate.

the convergence rate of the procedure. It should be said that at each iteration a control on the step length has been enforced to avoid feasible solutions being jumped over by the procedure.

Consideration of the acceleration graphs in Fig. 8 shows features that would be expected considering the nature of the experimental data and the characteristics of the identification model. The time lag shown in the figure, with elapsing time between identified and considered acceleration, is essentially due to the above mentioned features, that is constant period in one case and decreasing period in the other.

12. Identification results from the Solarino tests

In this section a synthesis of the analysis on all the Solarino tests is presented. Six free vibration tests with imposed initial displacement were performed on a base-isolated building in the town of Solarino in July 2004. The building considered has four stories and five floor slabs. These are identified by numbers from 0 (isolation floor) to 4 (roof). The second and third floors are close to the centre of mass of the building and the accelerations recorded on those floors are used in the present identification procedure. The results are shown in Table 4, with different backgrounds referring to tests performed in different days; the results shown with shaded background were performed in one day while those shown on white background were performed on another day a week later.

The identified frequencies and the corresponding periods match quite well whether obtained from data on the second floor or on the third floor. Also the damping ratios turn out to be quite similar in the same test whether obtained from data on one floor or on the other. The same can be said for the residual displacement and for the friction displacement. Some differences are however noticed from different tests conducted under similar initial displacements. There can be two reasons for these differences. The first one may be that the initial displacement is somehow uncertain because no record of the residual displacement was taken during the tests. Therefore the recorded initial displacement is not necessarily the true initial displacement. However, the residual displacement, especially for large initial displacements, should be only a small fraction of the imposed displacement and therefore the effect on the identified parameters should not be too large. Another reason for the differences noted may be temperature, which may have affected the transducer's calibration factor. In fact, the tests were performed in different hours of the day in two different days and the larger differences can be seen in similar tests performed in different days. The combination of these two factors may be responsible for the variability of the identified parameters. As it has been shown in Refs. [12,13] the results of the Solarino tests show a diminishing period with time; however the present model considers constant stiffness and consequently constant period. The periods identified with the present procedure from the tests and shown in Table 4 are generally slightly shorter than the first period from the tests. This is quite expected

Table 4
Identified parameters from tests on a Solarino building for the prescribed initial displacement $\hat{u}_0$

$\hat{u}_0$ (m)	u_{ad} (m)	u_r (m)	ζ	f_n (Hz)	T_n (s)
Acceleration recorded on floor 2					
0.1329	0.0033	−0.0096	0.1194	0.4314	2.32
0.1308	0.0026	−0.0106	0.1348	0.4298	2.33
0.1148	0.0027	−0.0122	0.1190	0.4315	2.32
0.1075	0.0017	0.0006	0.1494	0.4468	2.24
0.0967	0.0026	0.0048	0.1378	0.4472	2.24
0.0406	0.0030	−0.0024	0.1135	0.4879	2.05
Acceleration recorded on floor 3					
0.1329	0.0030	−0.0089	0.1219	0.4316	2.32
0.1308	0.0028	−0.0111	0.1305	0.4301	2.33
0.1148	0.0037	−0.0136	0.1055	0.4326	2.31
0.1075	0.0014	−0.0079	0.1534	0.4448	2.25
0.0967	0.0030	0.0060	0.1317	0.4462	2.24
0.0406	0.0029	−0.0016	0.1296	0.4916	2.03

Table 5
Identified stiffness and friction force in a Solarino building

Acceleration recorded on floor 2		Acceleration recorded on floor 3	
k (kN m^{-1})	f_{ad} (kN)	k (kN m^{-1})	f_{ad} (kN)
m = 1237 Mg			
9087	29.6	9096	27.2
9019	23.7	9032	25.7
9094	24.9	9137	34.1
9749	16.8	9662	13.7
9767	25.6	9722	29.1
11,626	34.5	11,801	34.0

because the larger displacements, velocities and accelerations occur in the first period and these are likely to affect the results considerably.

Additional information on the mechanical properties of the Solarino buildings may be obtained from the identified parameters in Table 4. In fact, if the mass of the building is known with reasonable accuracy, the identified frequencies may be used to evaluate the equivalent stiffness of the isolated building and from this the dynamic friction force may be calculated from the second of Eqs. (3). The mass identified in Ref. [13] is used to evaluate the equivalent stiffness and the dynamic friction force, shown in Table 5. The results are shown in the same order as in Table 4.

Considering that the design stiffness of the Solarino building was 9240 kN m^{-1} [12] and the experimental value from standard laboratory tests on two isolators was 9480 kN m^{-1}, the identified stiffnesses shown in Table 5 are quite accurate. The largest values correspond to a low amplitude test and are quite in line with the initial stiffness measured during the static phase preceding the free vibration test. It is interesting that the average value of the stiffness, calculated from the accelerations at the two floors considered, if the low amplitude test is excluded, provides an average value of 9337 kN m^{-1}, which is very close to the design value and to the experimental one. The average value of the dynamic friction force evaluated by excluding the low amplitude test and the anomalous results corresponding to the initial displacement of 10.75 cm turns out to be 25 kN. The Solarino buildings isolation system is composed of 12 high damping rubber bearings and of 13 sliding isolators [12,13]. By assuming that 50% of the weight affects the rubber bearings and that the other 50% affects the sliding isolators, it follows that the average dynamic friction coefficient is about 0.0041, in line with the values provided by the manufacturer for dimpled and lubricated PTFE. The estimated value for the friction coefficient must be intended only as a gross average value because the friction coefficient in sliding bearings depends significantly on several variables such as pressure, temperature, velocity and number of cycles of motion.

In conclusion it may be said that the parameters identified with the present procedure, from the knowledge of the floor acceleration and of the initial displacement, are of sufficient accuracy and in agreement with the values derived from laboratory tests. Also, the values of the equivalent viscous damping, appropriate to the high damping rubber bearings, are in good agreement with those derived via a different approach [13].

It may be of interest at this point to comment on the reason for the use in earthquake engineering of low friction sliding bearings in place of perhaps cheaper ones with a higher friction coefficient, which in turn would result in a higher energy dissipation capacity. While the fundamental period of vibration would not be changed by the higher friction force, a considerably higher shear force would be transmitted to the superstructure through the isolation system, producing higher damage. It may be worth mentioning that, if feasible and not conflicting with other functions, the ideal isolation system would be provided by a totality of perfectly sliding bearings which would keep the building still under the earthquake, with the ground moving below it. A convenient number of low friction sliders, combined with a complementary number of high damping rubber bearings, may be a useful compromise between ideal and reality.

13. Conclusions

A procedure for the identification in the frequency domain of structural systems with combined viscous and friction damping devices has been presented. The mathematical model used as the basis of the identification procedure considers constant stiffness and constant friction force. The response in the time domain and in the frequency domain of such a system to an imposed initial displacement has been derived in closed form. The response in the frequency domain, expressed as a summation of several terms, is used as the building blocks for the identification procedure. The least squares method is used to match the actual solution with a feasible solution in the solution space. It has been shown that the least squares method can find the actual (optimal) solution provided that this belongs to the search space. This demonstration was made by using a mathematical solution for the set of initial conditions and system parameters as the optimal solution and using a discrete sample of this solution as the experimental data to be identified. This experiment showed that the identification procedure works very well within a theoretical environment.

In real life experiments the sampled time history of the response is available rather than its Fourier Transform. Therefore, the first step to be taken is to derive the frequency response function from the recorded data using a Discrete Fourier Transform. Although this can be done efficiently using the Fast Fourier Transform algorithm, it turns out to be only an approximation, often a poor approximation, of what would be the real Fourier Transform of the actual solution. Fortunately, at least for systems with relatively low natural frequency, the match between Fourier Transform and Discrete Fourier Transform turns out to be quite good in a range of frequencies centred around the natural frequency of the system. This way of applying the identification procedure to simulate real life conditions proved to be quite reassuring. The distortion introduced by the DFT did not allow the exact solution to be obtained, but the approximate solution turned out to be quite accurate, at least within engineering uncertainties.

The next step has been to apply the procedure to the real Solarino tests. The ideal situation would be to have experiments on a structural prototype with the properties of the mathematical model considered. However, the authors used results obtained from tests on a real building which had been seismically retrofitted by base isolation. While it may be conceivable that the friction damping in the sliding bearings may somehow resemble the Coulomb friction damping, it is well known that the damping in the rubber bearings is quite complex and that high damping rubber bearings are better described by bi-linear models [20]. This is also confirmed by the available test data that show amplitude dependent periods. Nevertheless, the proposed identification procedure has been used with the available data to see whether reasonable results could still be obtained. These experiments are described in Section 10 and in Section 11.

In Section 10, in order to obtain better results, the identification procedure has been adjusted assuming the initial displacement to be known instead of being a parameter to be identified. In principle, even the residual displacement could be considered as a test datum and it may be argued that the results of the identification could be improved further in this case. The analysis of the identification results in the time domain shows that the first cycle of motion is identified better than the following ones and that the time gap between recorded and identified response tends to increase with increasing number of cycles. Natural frequency, damping ratio and dynamic friction displacement seem to yield reasonable values. The identified parameters seem to be more appropriate to the first cycle of motion than to the subsequent ones.

In Section 11, all the available dynamic Solarino tests are considered, using the horizontal accelerations recorded on two floors supposedly close to the centre of mass of the building. The six dynamic tests were performed in two different days, three in each day, and at different hours of the day. Some differences may be noticed in the identified parameters from tests with similar imposed initial displacements performed in different days. The possible reasons for those differences have been discussed. Overall the identified parameters appear to be sufficiently reliable and in reasonable agreement with the values obtained with other methods.

Looking to the future, an important aspect to be considered is that the mathematical model used as a basis for the identification procedure does not quite match a realistic physical model for the building. This appears to suggest the use of a different identification procedure, with a better model, directly in the time domain. Nevertheless, the results obtained are quite encouraging and it would seem worthwhile to repeat the tests or to perform other tests measuring accurately some measurable parameters such as the initial and the residual

displacement. These new tests could be used to crosscheck the results of the present procedure and those obtainable from a more accurate model and identification procedure in the time domain. It would also be worth considering whether physical systems accurately described by the current model really do exist or may be built without too much difficulty.

References

[1] R.W. Clough, J. Penzien, *Dynamics of Structures*, Mc-Graw-Hill, Inc., New York, 1975 1993.
[2] A.K. Chopra, *Dynamics of Structures: Theory and Applications to Earthquake Engineering*, Prentice-Hall, Englewood Cliffs, NJ, 2001.
[3] D.J. Ewins, *Modal Testing: Theory and Practice*, Research Studies Press, England, 1984.
[4] E. Balmès, Frequency domain identification of structural dynamics of structural dynamics using the pole/residue parametrization, *Proceedings of the 14th IMAC*, Dearbon, MI, 1996, pp. 540–546.
[5] E. Balmès, New results on the identification of normal modes from experimental complex modes, *Mechanical Systems and Signal Processing* 11-2 (1997) 229–243.
[6] E. Balmès, Structural Dynamics Toolbox, User's Manual 3.0, Scientific Software Group, Sèvres, France.
[7] J.-W. Liang, Damping estimation via energy-dissipation method, *Journal of Sound and Vibration* 307 (2007) 349–364.
[8] Z. Wu, et al., Identification of non-linear viscous damping and Coulomb friction from the free response data, *Journal of Sound and Vibration* 304 (2007) 407–414.
[9] Graeme Haynes, McVerry, Frequency domain identification of structural models from earthquake records. Technical Report: CaltechEERL:1979, EERL-79-02, California Institute of Technology, 1979.
[10] Graeme Haynes, McVerry, James L. Beck, Structural identification of JPL Building 180 using optimally synchronized earthquake records. Technical Report: CaltechEERL:1983, EERL-83-01. California Institute of Technology, 1983.
[11] H. Lus, R. Bettian R.W. Longman, Identification of Linear Structural Systems Using Earthquake Induced Vibration Data, *Earthquake Engineering and Structural Dynamics* 28 (1999) 1449–1467.
[12] G. Oliveto, M. Granata, G. Buda, P. Sciacca, Preliminary results from full-scale free vibration tests on a four story reinforced concrete building after seismic rehabilitation by base isolation, *JSSI 10th Anniversary Symposium on Performance of Response Controlled Buildings,* Yokohama, Japan, 2004.
[13] G. Oliveto, G. Scalia, Free-vibration tests following seismic retrofitting by base isolation on the Solarino buildings, *Proceedings of the Eighth US National Conference on Earthquake Engineering*, San Francisco, 2006, Paper No 1254.
[14] N. Kani, M. Takayama, A. Wada, Performance of base isolated buildings in Japan, *Proceedings of the Eighth US National Conference on Earthquake Engineering*, San Francisco, 2006, Paper No. 2181.
[15] M. Tamari, T. Tokita, S. Kawamoto, T. Komuro, H. Fukuyama, M. Iiba, Performance of a seismic isolated building in the 2004 Niigata-Ken Chuetsu Earthquake, *Proceedings of the Eighth US National Conference on Earthquake Engineering*, San Francisco, 2006, Paper No. 815.
[16] M. Seki, M. Miyazaki, Y. Tsuneki, K. Kataoka, *A Masonry School Building Retrofitted by Base Isolation Technology*, 12WCEE, 2000.
[17] G. Oliveto, G. Scalia, *Wavelet Identification of Base Isolated Buildings: Application to the Solarino Buildings*, ANIDIS 2007, Pisa, Italy.
[18] N.D. Oliveto, *Modelli semplificati per l'isolamento alla base e simulazione delle prove di Solarino, Tesi di Laurea*, Dipartimento di Ingegneria Civile e Ambientale, Università di Catania, Luglio, 2006.
[19] D.E. Newland, *An Introduction to Random Vibrations, Spectral & Wavelet Analysis*, Longman Group Limited, Harlow, UK, 1995.
[20] F. Naeim, J.M. Kelly, *Design of Seismic Isolated Structures*, Wiley, New York, 1999.